Multiple two-photon targeted whole-cell patch-clamp recordings from monosynaptically connected neurons in vivo

Running title: Multiple whole-cell recordings in vivo

Jean-Sébastien Jouhanneau[1,2] and James F.A. Poulet[1,2]*

[1]Department of Neuroscience, Max Delbrück Center for Molecular Medicine (MDC), Berlin-Buch, Germany.
[2]Neuroscience Research Center and Cluster of Excellence NeuroCure, Charité-Universitätsmedizin Berlin, Germany.

*Correspondence to be addressed to:
James Poulet,
Max Delbrück Center for Molecular Medicine (MDC),
Robert-Rössle-Str. 10,
10392 Berlin-Buch,
Germany.

Telephone: +49 (0)30 450 639795
Fax: +49 (0)30 450 539979
E-Mail: james.poulet@mdc-berlin.de
Website: http://www.mdc-berlin.de/poulet

Abstract

Although we know a great deal about monosynaptic connectivity, transmission and integration in the mammalian nervous system from *in vitro* studies, very little is known *in vivo*. This is partly because it is technically difficult to evoke action potentials and simultaneously record small amplitude subthreshold responses in closely (< 150 µm) located pairs of neurons. To address this, we have developed *in vivo* two-photon targeted multiple (2 – 4) whole-cell patch clamp recordings of nearby neurons in superficial layers 1 to 3 of primary somatosensory cortex. Here we describe a step-by-step guide to this approach in the anesthetised mouse, including: the design of the setup, surgery, preparation of pipettes, targeting and acquisition of multiple whole-cell recordings, as well as in vivo and post-hoc histology. The procedure takes ~ 4 hours from start of surgery to end of recording and allows examinations both into the electrophysiological features of unitary excitatory and inhibitory monosynaptic inputs and the synaptic mechanisms of correlated neuronal activity.

INTRODUCTION

Monosynaptic transmission underpins action potential generation and the flow of information within neural circuits. Over the last decades, *in vitro* approaches have provided an enormous amount of data on the connectivity rates and the electrophysiological and anatomical properties of synapses. In the intact brain, however, synapses function during different behavioural and network states as well fluctuating levels of neuromodulators and far less is known about monosynaptic transmission and the activity of connected neurons in vivo.

In vivo approaches to identify connected pairs of neurons in the mammalian nervous system have typically performed electrophysiological recordings of multiple single neurons and examined the average response of one neuron to spontaneously occurring action potentials in another neuron. “Spike triggered averaging” of cortical neurons has been performed both with multiple extracellular recordings (Bartho, 2004; Csicsvari et al., 1998; English et al., 2017; Fujisawa et al., 2008; Reid and Alonso, 1995; Swadlow and Gusev, 2002) and a combination of extracellular and intracellular membrane potential recordings (Bruno, 2006; Crochet et al., 2005; London et al., 2010; Matsumura et al., 1996; Yu and Ferster, 2013). However, because it is not yet possible to record the activity of all neurons presynaptic to the cells of interest and cortical neurons can fire simultaneously, it is difficult to confirm whether correlated activity is the result of a direct synaptic connection between the two recorded neurons or input from a third, unrecorded, neuron with similar firing dynamics. One approach to get around the problem of synchronous input is to have experimental control of action potential timing using single cell stimulation, while simultaneously recording the evoked membrane potential response from a second neuron. While, care has to be taken in concluding that any synaptic response is the result of a monosynaptic rather than polysynaptic input (Berry and Pentreath, 1976; Parker, 2010), this approach has been used in vivo to characterise the wiring and functional properties of synaptic connections in a number of non-mammalian species (Burrows, 1996; Parker, 2003; Poulet and Hedwig, 2006; Roberts et al., 2010).

Mapping the synaptic properties and monosynaptic connectivity rates in neocortex has been a central aim of in vitro slice studies, with visually guided multiple whole-cell patch clamp membrane potential recordings being the method of choice (Deuchars and Thomson, 1995; Edwards et al., 1989; Feldmeyer and Radnikow, 2016; Feldmeyer et al., 2006; Geiger et al., 1997; Lalanne et al., 2016; Lefort et al., 2009; Markram et al., 1997; Mason et al., 1991; Wozny and Williams, 2011; Yassin et al., 2010).The whole-cell recording technique has been adapted for use in vivo (Lee and Brecht, 2018; Margrie et al., 2002; Petersen, 2017) with more recent studies using dual, blind, whole-cell recordings to assess correlations of sub- and supra-threshold V_m activity between pairs of cortical neurons (Arroyo et al., 2018; Gentet et al., 2010; Poulet and Petersen, 2008; Zhao et al., 2016). While dual membrane potential recordings provide a technical basis for testing for monosynaptic connectivity, the likelihood of two cortical

neurons being connected is low, dependent on cell type and negatively correlated with inter-somatic distance (Holmgren et al., 2003; Perin et al., 2011). Therefore, to identify connected pairs of neurons in vivo, it would help to be able to record from nearby, genetically labelled neurons using visual control.

Here we describe a new approach using in vivo two-photon microscopy to target whole-cell recordings to neighboring, fluorescently labelled layer 2/3 cortical neurons. We show that this technique can be used to evoke action potentials and isolate unitary excitatory and inhibitory postsynaptic potentials in postsynaptic neurons (Ferrarese et al., 2018; Jouhanneau et al., 2015; 2018). A troubleshooting table is provided (**Table 1**) and we go on to discuss potential improvements and future applications of this technique in assessing the link between monosynaptic transmission and cortical function.

MATERIALS AND METHODS

The aim of this article is to provide a description of multiple, 2-photon targeted patch-clamp recordings to monitor monosynaptic connectivity in vivo. The procedure is described for an acute one-day experiment in anaesthetised mice. All experiments were performed according to protocols approved by the Berlin Animal Ethics committee (Landesamt für Gesundheit und Sociales, LAGeSo) and comply with the European animal welfare law.

Two-photon microscope

In vivo two-photon microscopy with galvanometric scanning (Femto2D, Femtonics) is used to visualize neurons and the whole-cell recording pipettes (**Figure 1**). Two, photomultiplier tubes (PMTs) (Hamamtsu GasAsP detectors) are used to detect light, one fitted with a 498 – 570 nm band pass filter and the second with a 598 – 700 nm filter to enable detection of green and red fluorophores respectively. A CCD camera is coupled to the microscope and used at the start of the experiment to place the electrodes over the region of interest using a 4X objective (Olympus UPLFLN 4X, NA 0.13, W.D 17 mm). Subsequently a 40X water immersion objective with a long working distance (Olympus LUMPLFLN 40XW, NA 0.8, W.D 3.3 mm) is used to target cell soma of interest. The tuneable (680 – 1080 nm), mode-locked Ti:Sapphire laser (Chameleon Ultra II, Coherent) is used to excite a wide range of fluorophores (eg GFP, Alexa 488, Alexa 594, tdTomato). The Pockel cell (E.O. Modulator, Conoptics) enables a fine control of the laser beam intensity and prevent tissue damage. All these devices are controlled by a Matlab (mathworks) based imaging data acquisition software (MES v4.0 software, Femtonics).

Mice

The technique works with both wild type mice and strains expressing fluorescent proteins in subsets of neurons. In this article, we used mice aged between P18 – P30 from C57bl6J, NEX-cre (Goebbels et al., 2006) x Ai9 (Madisen et al., 2010), fosGFP (Barth et al., 2004), GAD67-GFP (Tamamaki et al., 2003), PV-cre (Hippenmeyer et al., 2005) x Ai9, or SST-cre (Taniguchi et al., 2011) x Ai9 background. Mice were maintained on a 12h light – dark cycle and had food and water *ad libitum*.

Surgery

To expose the brain for recordings, mice are first anesthetised with 1.5% isoflurane and show an absence of tail pinch reflex and whisker movements. Eye ointment (Bei trockenen Auge, Visidic) is used to protect the eyes and body temperature is maintained at 36ºC using a closed loop system with rectal probe and heating pad (DC Temperature controller, FHC). All tools are cleaned and dry heat sterilized using hot glass beads steriliser (Steri 250, Keller, Fine Science Tools) prior to surgery. The head is shaved and 70% alcohol followed by iodine solution are

applied before performing the first skin incision. If necessary, intrinsic optical imaging through the skull can be performed at this stage if functional localisation of recording site is required. The conjunctive tissue is next carefully removed using forceps and micro-scissors (Fine science Tools) and the skull is cleaned using a microcurette (Fine science Tools) to remove any remaining tissue on the surface of the bone. 3% hydrogen peroxide (H_2O_2) solution can be applied for 30 seconds at this stage to help clean the exposed bone surface, however the bone can also be cleaned by gently scraping the bone with a razor blade. Next the skull is washed thoroughly with Ringer's solution (135 NaCl, 5 KCl, 5 HEPES, 1.8 $CaCl_2$, and 1 $MgCl_2$135 NaCl, 5 KCl, 5 HEPES, 1.8 $CaCl_2$, and 1 $MgCl_2$) and thoroughly dried. Avoiding the recording site, the exposed skull is then lightly scratched with a 25G syringe needle to create grooves in the skull. It is important to remove any remaining hairs or dirt at this stage to avoid possible infection. Next, superglue (Loctite 401) is applied first at the edges of the exposed skull, to glue the skin to the bone, and then to the entire exposed skull surface avoiding the recording site. A lightweight metal head implant is then placed on the hemisphere contralateral to the recording site and covered with glue. To secure the head implant, dental cement is applied on top of the entire layer of glue. As the dental cement viscosity increases, a recording chamber with access for the recording pipettes can be modelled around the area of interest using a spatula. It is important to completely cover the head implant with glue and dental cement to avoid any possible contact between the Ringer's solution and the metal of the head implant during the recording which can lead to electrical noise and voltage offsets.

Once hardened, the recording chamber is filled with Ringer's solution. After a few minutes, the skull will become translucent and the blood vessels visible. Then, the Ringer's solution should be removed to let the bone dry and a 500 µm diameter dental drill head (Komet, Brassler) operated by a dental drill (Success 40, Osada) is used to thin the skull over the recording site. Drilling is stopped as soon as blood vessels become clearly visible through the bone. This corresponds to a bone thickness of ~ 100 µm (Papadopoulos et al., 2017). Bone dust is removed with wet tissue paper and the chamber is refilled with Ringer's solution. A 27G syringe needle is used to pick away the final layer of bone with great care. Next, a duratomy is made using a 25G needle with a handmade small hook at the tip of the needle. Adjusting the angle of illumination of the craniotomy is key to visualizing the dura (~ 30º). The handmade hooked-tip of the needle is used to gently lift the dura away from the future spot of pipette insertion.

Whole-cell pipettes and electrophysiological equipment

We use a four-step pulling custom program on a Sutter puller (Model P-1000, Sutter instrument) with 2 mm diameter borosilicate capillaries (Hilgenberg) to pull 5 – 7 MΩ pipettes. The first two lines of the pulling program are identical and used to create a taper of ~ 6 mm

165 and a tip of ~ 2µm (**Figure 1E, F**), while the third and fourth step are used to decrease the
166 diameter and defining the tip shape and resistance. Three to four pipettes are filled with
167 intracellular solution containing, in mM: 135 potassium gluconate, 4 KCl, 10 HEPES, 10
168 phosphocreatine, 4 MgATP, 0.3 Na3GTP (adjusted to pH 7.3 with KOH), 25 µm Alexa-594
169 (Invitrogen) and 2 mg/ml biocytin. Pipettes are next fixed to a pipette holder (Molecular
170 Devices) mounted on a LN Junior 3-axis (X, Y, and Z) micromanipulator with low drift and a
171 long traverse path (up to 22 mm on the X axis) where the X axis is angled at 35 – 40º (**Figure**
172 **1D**) (Luigs and Neumann). An Ag/AgCl ground electrode is next placed into the recording
173 chamber filled with Ringer's solution and electrophysiological signals are amplified using the
174 Axon Instruments amplifier Multiclamp 700B (Molecular Devices). The analog signals recorded
175 are filtered at 10 kHz and digitized at 20 kHz using the analog/digital converter ITC-18 board
176 (Heka) and IgorPro (Wavemetrics) running on a Windows PC. For online visualization of the
177 electrophysiological signal we use an oscilloscope (Tektronix TDS2024C) with a max sample
178 rate 2 GS/s. To allow easier and faster access to the exposed brain, all pipettes are positioned
179 on one side of the preparation (**Figure1B**).
180
181 **Multiple two-photon targeted whole-cell patch clamp recordings**
182 As soon as the pipettes are mounted on the holders a 180 – 200 mbar positive pressure is
183 applied via a syringe. A manual-seal-sucker (Sigmann Elektronik GmbH) manometer is used
184 to monitor the pressure applied to all channels independently. All electrodes are moved into
185 the Ringer's solution in the recording chamber in voltage-clamp seal-test mode to monitor the
186 pipette tip resistance on the oscilloscope.
187
188 **Step 1: Positioning above brain (Figure 2A).** Using the low magnification 4X objective and
189 the CCD camera, the pipettes are lowered (~ 20 – 30µm apart) until they are ~300 µm above
190 the region of interest. Then, by switching to the higher magnification 40X objective the pipettes
191 are moved to the same focal plan. The position of the pipettes is recorded. A clean entry of the
192 pipette into the brain is a critical indicator of successful future patching, so special care is taken
193 to examine the brain surface and identify clear entry points without large blood vessels, dirt or
194 irregular surfaces. The coordinates of the insertion point are noted and the focus is moved
195 back up to the pipette tips which are then carefully aligned. The focal plan is next moved to the
196 brain surface and the pipettes are lowered vertically using the Z-axis one by one using a
197 medium control sensitivity of the micromanipulator control pads (28 µm per handwheel
198 rotation). As the pipettes are lowered, slight lateral movements are performed to help visualize
199 the tips. Because of the positive pressure applied to the pipette, a clear depression on the
200 brain surface is seen as soon as the pipette gets closer to the brain. At this point, the

micromanipulator values are reset to zero. At the same time, the resistance of the pipette should increase (as observed by a decrease in the current step amplitude on the oscilloscope).

Step 2: Entering the brain (Figure 2B). Subsequently, using the highest sensitivity speed on the micromanipulator (3 µm per handwheel rotation), the pipettes are moved through the pia one by one. As soon as the electrodes pass through the pia and enter the brain, as signalled by a reduction in resistance with a subsequent sudden relaxation to the initial pipette resistance value, the pressure is reduced down to 70 – 90 mbar and the pipette tips moved to – 50 µm depth using X-axis. Two-photon imaging is used as soon as the pipettes are in the brain. Because of the positive pressure the dye, Alexa-594, contained in the intracellular solution will diffuse into the neuropil and highlight blood vessels, cell soma and dendrites as dark "shadows".

Step 3: Targeting cells of interest (Figure 2C). Having lowered the pressure to 70-90 mbar, using the same speed of 3 µm per handwheel rotation, the pipettes are moved one by one to a depth of – 150 to – 200 µm (boarder of cortical layers 1 and 2). During pipette movement great care is taken to avoid cells bodies and capillaries using both visual control from the two-photon imaging and the seal test pulse on the oscilloscope. In wild-type mice, without expression of fluorescent proteins, the contrast between the dye in the neuropil and the dark unlabelled cells, the shadow patching technique (Kitamura et al., 2008) can be used to target neurons of interest. With experience, the dendritic shape of the cell can help identify excitatory from inhibitory neurons. A maximum of 100 µm of lateral movement per pipette is allowed but the less the better. Then the pressure is decreased to 30 mbar and the micromanipulator controller's pads switched to a stepping mode (2 µm per step).

Step 4: Sealing (Figure 2D). Next, the final approach and seal is performed sequentially, one pipette at a time. The pipette voltage offset is set to 0 mV and the first pipette tip is lowered using 2 µm steps onto the cell membrane using the X-axis while watching the oscilloscope closely to observe changes in tip resistance. A sign of a good contact between the pipette tip and the neuron occurs when the seal test pulse reduces in amplitude and fluctuates with a wave like pattern. In contrast, an abrupt and sustained reduction in pulse amplitude without fluctuations is typical of a contact with a capillary. Good contact can sometimes be visualised during two-photon scanning as a small, expanding, fluorescent dimple in the cell membrane. As soon as a good first contact has been observed, one or two further steps are made and the positive pressure immediately released followed by a transient negative pressure to optimise the seal. V_m holding voltage is immediately placed at – 70mV to help improve seal. Typically, this leads to a large reduction in the amplitude of the test pulse and the formation of a giga-

238 seal, however light manual suction is sometimes required to improve the quality of the seal
239 and/or transiently hyperpolarizing the cell to – 100mV. This procedure is then repeated with
240 the other pipettes one after the other.
241
242 **Step 5: Whole-cell configuration (Figure 2E).** When all the pipettes are sealed onto the
243 targeted neurons, a brief and gentle suction is used to break the membrane and enter whole-
244 cell configuration on each of the neurons with a giga-seal. With the whole-cell configuration
245 established, we next retract each pipette away from the cell body ~ 5 µm using the X axis used
246 for the final approach to the cell, and the wheel at the lowest speed on the micromanipulator
247 pads. All recordings are then switched to current clamp mode for membrane potential
248 recordings.
249
250 **Current injection**
251 After allowing the cells to recover (~ 2 – 3 min), we next use intracellular current stimulation
252 protocol to characterize their intrinsic properties. In our experiments, each neuron receives
253 500 ms square current injections ranging in amplitude of – 200, – 100 pA, and then 50, 100,
254 150, 200 pA. This helps define rheobase, intrinsic excitability, and firing pattern of the recorded
255 neurons. Next, hyperpolarizing current pulses of – 100 pA, 200 ms duration, 200 ms interval,
256 are applied for 30 s to determine the input resistance and access resistance (ideally < 50 MΩ),
257 followed by 30 s without stimulation to record spontaneous sub- and supra-threshold activity.
258 Then, we define the square current pulse amplitude necessary to drive the recorded neuron to
259 fire a single action potential. We aim to use the smallest duration possible, usually 10 to 20 ms
260 of 100 to 400 pA amplitude. When these parameters have been set we repeat this stimulus for
261 each cell at 0.5 or 1 Hz to trigger single action potential (**Figure 3B**). To study synaptic
262 dynamics using pair of action potential to define pair pulse ratio we increase the current
263 injection time to ~50 ms (for more details see (Jouhanneau et al., 2015)).
264 There was no tonic current injection applied during the recording to avoid misestimation
265 of the V_m due to possible changes in the access resistance during the recording. Recordings
266 are terminated when the most hyperpolarized sections of the Downstate V_m are more
267 depolarized than – 50mV. Due to differences in ionic concentration, valency and mobility
268 between the intracellular and extracellular solution, a Liquid Junction Potential (LJP) will be
269 established when the pipette enters the recording chamber (Barry and Lynch, 1991). The LJP
270 can be ~ 10 mV and is complex to calculate accurately in vivo, therefore to avoid
271 miscalculation, we do not subtract the LJP from the recorded values.
272
273 **Anatomy: live fluorescent two-photon imaging and post hoc biocytin staining**

274 During a successful recording, Alexa fluorophore 594 diffuses into the neurons and allows live
275 visualization of the cell's anatomy (**Figures 2E, 3A and 3D**). Stacks of scans at 820 nm
276 wavelength separated by 2 µm can help identify the cell type using the somatic and dendritic
277 anatomy as well as the presence of dendritic spines. However, for higher resolution anatomical
278 reconstruction mice are deeply anaesthetized with an i.p. injection of urethane (2.5 g/kg,
279 Sigma-Aldrich) before being transcardially perfused with cold Ringer's solution and then by 4%
280 paraformaldehyde solution (PFA, Roti-Histofix 4%, Roth). After perfusion, the brain is removed
281 and placed in 4% PFA overnight at 4ºC and then in phosphate buffer (Roti-CELL 10xPBS,
282 Roth) and stored at 4ºC until further processing.
283 Tangential slices of 100 µm are cut using a Leica VT1000 S vibratome and stored in
284 phosphate buffer. Intracellular staining with biocytin is then revealed using a standard ABC kit
285 (Vectastain Elite ABC-Peroxidase kit, Biozol), with diaminobenzidine (DAB, Vector lab)
286 enhancement. Treated slices are mounted on glass slides using a gel mounting agent (Moviol,
287 Sigma-Aldrich), sealed with nail polish and stored at 4ºC. Reconstructions of the recorded
288 neurons are performed using the software NeuroLucida (MicroBrightField).
289
290 **Success rates**
291 We next calculated the success rates of our approach during patching of layer 2 neurons
292 (depth: -182.01 +/- 2.49 µm; distance: 38.99 +/- 1.84 µm) in 37 trials, each trial corresponding
293 to one insertion of 3 pipettes into the brain, in 15 anesthetised wild-type mice (males, 21.97 +/-
294 0.25 days old) using the shadow patch method performed by a trained researcher. We
295 calculated the number of times we were unsuccessful or obtained a single, dual or triple whole-
296 cell recording. In 17/37 trials we obtained a triple recording, in 17/37 trials a dual, in 2/37 single
297 and in 1/37 no recordings (**Figure 2G**). Thus in 92% of shadow patching trials using three
298 pipettes we obtained at least a dual recoding that would allow a connectivity test. We then
299 repeated this analysis for attempted triple recordings (3 pipettes) in mice expressing a
300 fluorescently labelled indicator in a subset of GABA-ergic interneurons (PV-tdT or SST-tdT),
301 where a successful recording trial had to include a least one fluorescently labelled neuron. In
302 11/41 trials from 18 mice we obtained a triple recording, in 15/41 trials double, 8/41 single (ie
303 one td-T labelled neuron recorded) and were unsuccessful in 7/41 attempts (**Figure 2G**). Thus,
304 in 63 % of trials with fluorescently labelled mice we obtained at least a dual recording including
305 1 fluorescent GABA-ergic neuron to allow for a connectivity test.
306 During these experiments, we noticed that for trials that took longer it seemed harder
307 to perform a successful whole-cell recording. From our triple recording dataset in Figure 2, we
308 therefore systematically recorded the time to go from Step A (positioning above brain) to Step
309 E (whole-cell recording). Plotting the time taken against the success rates of successfully
310 patching one neuron showed a significant negative correlation and confirmed that reducing the
311 time taken to patch improves success rates for patching. In a different set of experiments where

312 the recordings were not terminated prematurely and the Downstate V_m was < – 50 mV, we
313 calculated a mean recording time of 14 minutes 54 seconds +/- 6 minutes 7 seconds (n = 143
314 cells) with a minimum recording time of 5 minutes and a maximum of 32 minutes.
315
316 **In vivo glutamatergic excitatory monosynaptic inputs to excitatory pyramidal neurons**
317 **and GABA-ergic inhibitory interneurons**
318 During slow wave sleep and under anaesthesia the membrane potential of cortical neurons
319 fluctuates between hyperpolarized, synaptically quiescent, Downstates and depolarized,
320 synaptically active, Upstates (Steriade et al., 1993). We first examined synaptic transmission
321 between excitatory pyramidal neurons in Downstates. In wild type mice, pyramidal neurons
322 were targeted using their pyramidal shaped soma and apical trunk visible as shadows against
323 the fluorescent extracellular space and after each successful recording, confirmed using Z-
324 stack images to visualise the somatic and dendritic morphology (e.g. spines). Moreover, we
325 used transgenic mice expressing fluorophore in excitatory neurons using offspring of the NEX-
326 cre line crossed with the Ai9 YFP reporter mouse to study excitatory pyramidal neurons (PYR)
327 to PYR monosynaptic connectivity. To trigger spikes and measure synaptic transmission we
328 depolarized each neuron with injection of a short depolarising current 100 – 400 pA of 20 – 50
329 ms duration at 0.5 Hz to evoked a single action potential (**Figure 3B**) and used spike trigger
330 averages to look at the corresponding unitary excitatory postsynaptic potential ($_u$EPSP). To
331 study short term synaptic dynamics, further action potentials could be triggered by longer
332 current pulses or by trains of shorter pulses**.** For further details on the properties of the
333 connections see (Jouhanneau et al., 2015).
334 We went on to use the same approach to examine excitatory connections from PYRs
335 to different subtypes of GABA-ergic neurons including parvalbumin (PV), somatostatin (SST)
336 and vasoactive intestinal polypeptide (VIP) expressing neurons. The PV-cre, SST-cre and VIP-
337 cre mice were crossed with the Ai9 reporter line to visualise the subpopulation of GABA-ergic
338 neurons of interest. The approach to target recordings of interneurons is technically similar to
339 that of excitatory neurons. However, in some cases, during the sealing step, the positive
340 pressure was lower than usual (~ 10 mbar) in order to target small diameter neurons like VIP
341 interneurons**.** For further details on inputs to PV and SST interneurons in vivo see (Jouhanneau
342 et al., 2018).
343
344 **Inhibitory monosynaptic connections to PYRs and INTs in vivo**
345 We next used multi-patch targeted recordings to examine inhibitory monosynaptic
346 neurotransmission in vivo. Here we recorded inhibitory connections from GABA-ergic INTs to
347 PYRs and also from INT to INT. The recording procedure is similar to that described above,
348 but because interneurons often have a higher input resistance, less positive current is typically

349 used to trigger single action potentials. Moreover, because of their hyperpolarized reversal
350 potential, $_u$IPSPs are more visible at more depolarized V_m values. This was evident in our
351 recordings, where the amplitude of $_u$IPSPs was larger in Upstates compared to Downstates
352 (Jouhanneau et al., 2018).
353

DISCUSSION

Understanding the link between monosynaptic connectivity and the functional properties of cortical neurons is a key goal of neuroscience. Here we have described an approach that allows V_m recordings of monosynaptically connected cortical neurons in vivo. The setup uses a standard in vivo two-photon microscope, whole-cell patch clamp amplifiers and motorised micromanipulators. With training, multiple whole-cell recordings of neurons in layer 2 can be performed with a success rate of forming a dual recording of ~ 90% and recording duration (~ 15 mins) similar to single electrode blind in vivo patch clamp recordings. In **Table 1** we have outlined a list of common problems with targeted patch clamp recordings and possible solutions. Future studies could now use this method to assess cell-type specific synaptic connectivity in vivo and the synaptic mechanisms of correlated cortical spiking.

Recent results using in vivo targeted whole-cell recordings of synaptically connected neurons

Because of tissue slicing and differences in neuromodulator and extracellular ion concentrations, it was unclear whether basic properties of excitatory connections would be similar in the living animal as compared to prior cortical slice work. Therefore, in a first study, we used two-photon targeted multiple whole-cell recordings to examine glutamatergic monosynaptic transmission between layer 2 pyramidal neurons (Jouhanneau et al., 2015). Overall, we observed that the rates of connectivity, the amplitude and kinetics were similar to in vitro studies in this cortical region (Feldmeyer et al., 2006; Lefort and Petersen, 2017) with layer 2 excitatory neurons connected by non-random, sparse, small amplitude connections.

Cortical neurons in vivo are constantly active with action potentials generated during depolarized phases of spontaneous synaptic activity. The impact of the network activity on synaptic transmission, however, has been debated (Bruno, 2006; Crochet et al., 2005; Destexhe et al., 2003; Pala and Petersen, 2014; Reig et al., 2015), in part because of the lack of methods to record from synaptically connected neurons in vivo. Recently, two studies investigated the impact of slow network activity on monosynaptic transmission in anaesthetized and awake resting mice (Ferrarese et al., 2018; Pala and Petersen, 2014). Despite the 10 – 15 mV depolarization during a depolarized phase of slow activity, there was little modulation in the $_u$EPSP amplitude at the population level (Ferrarese et al., 2018; Pala and Petersen, 2014). However, we observed that smaller (< 400uV) amplitude inputs are increased in amplitude during periods of depolarized V_m, whereas larger amplitude inputs are decreased (Ferrarese et al., 2018). We went on to use intracellular pharmacology to show that this amplification effect was mediated by postsynaptic voltage gated ion channels. Interestingly, recent work in awake animals using single cell optogenetic stimulation has shown an increase in $_u$EPSP amplitude during periods of movement compared to periods of quiet

391 wakefulness (Pala and Petersen, 2018). Further work is required to understand the
392 mechanisms underlying this increase, but one possibility is that it is the result of
393 neuromodulatory inputs to cortex during movement (Urban-Ciecko et al., 2018).
394 Spike triggered averaging of the V_m of excitatory L2/3 cortical pyramidal neurons has
395 shown large amplitude and cell-specific pre-spike depolarizations (Poulet and Petersen, 2008;
396 Zhao et al., 2016), indicating that summation of many inputs are and/or non-linear dendritic
397 events are required to drive spiking in excitatory neurons in vivo. Indeed, we were unable to
398 evoke APs in excitatory neurons with $_u$EPSPs, even during depolarized Upstates (Jouhanneau
399 et al., 2018). In contrast, GABA-ergic interneurons show smaller amplitude pre-spike
400 depolarizations (Gentet et al., 2010), and, using the multi-patch approach, we showed that
401 single excitatory synaptic inputs can trigger action potentials in PV-expressing GABA-ergic
402 neurons during Upstates (Jouhanneau et al., 2018). This difference was the result of a
403 combination of larger amplitude and faster rising inputs to PV neurons as well as an overall
404 more depolarized V_m during Upstates. Single excitatory input evoked spiking in PV neurons
405 led to fast disynaptic inhibition of neighbouring pyramidal neurons and may contribute to their
406 sparse firing rates.
407
408 **Limitations, uses and possible improvements**
409 The success rates of obtaining a visually targeted whole-cell recording is strongly dependent
410 on the cleanliness of the tip of the pipette. In addition, we noted that clean removal of the dura
411 and entering the brain at a clean entry point devoid of dirt were important aspects of a
412 successful experiment. Likewise, the longer the time to patch a neuron the lower the likelihood
413 of success (**Figure 2**).
414 Increasing the number of pipettes per trial helps test more possible connections giving
415 the opportunity to look at higher order connectivity motifs (Guzman et al., 2016; Peng et al.,
416 2017) and provides the experimenter with a higher chance of obtaining a dual recording. While
417 we have successfully used 4 pipettes to obtain quadruple whole-cell recordings (**Figure 2A-**
418 **E**), our data on success rates (**Figure 2G-H**) was taken from a series of experiments using 3
419 pipettes. During wildtype shadow patching, the extra time to use 4 rather than 3 is not
420 considerable and can be a significant advantage to increase the yield recorded cells. However,
421 for targeting fluorescently labelled subsets of neurons, the experimenter needs to weigh the
422 advantage of using a 4th pipette against the extra time taken to insert 4 pipettes into the brain.
423 A limitation of the method described above is the use of anaesthesia during the
424 recording session. An important future aim is therefore to perform this technique in awake and
425 behaving animals. While multiple whole-cell recordings have been performed in awake animals
426 (Arroyo et al., 2018; Gentet et al., 2010; Poulet and Petersen, 2008; Zhao et al., 2016), little
427 data exists on synaptic transmission in awake animals (Pala and Petersen, 2018). In part this

428 is because of worse control of the mechanical stability of the brain during behavior. However,
429 the use of agarose or cover slips on the brain surface has helped reduce movement for imaging
430 experiments and trackball systems have helped reduce pressure exerted on the head during
431 leg movements may help stabilise the brain and allow recordings in behaving mice.

432 The method and data presented above has focussed on closely positioned (< 150 µm
433 apart) neurons in superficial layers of neocortex. It would, of course, be interesting to examine
434 synaptic transmission between deeper layer neurons or between neurons positioned further
435 apart, perhaps even in different cortical regions; something not easy to achieve in brain slice
436 studies. Electrodes can easily be positioned to target different parts of the brain, but both the
437 recording depth and field of view are determined by the optical properties of the microscope.
438 The combination of cell type specific mouse lines (Daigle et al., 2018; Gerfen et al., 2013;
439 Harris et al., 2014) with improved depth resolution 2-photon microscopes (Papadopoulos et
440 al., 2017) allows optical access to granular and subgranular layers and may make multiple
441 recordings possible in deeper layers. Moreover, new two-photon microscope designs with
442 larger fields of view could provide the possibility to examine neurons situated 1000s of microns
443 apart (Sofroniew et al., 2016).

444 Cortical excitatory neurons are sparsely connected and therefore a key limitation to the
445 throughput of any connectivity study is identifying connected pairs of neurons. Both in vitro and
446 in vivo studies are normally made blind to connectivity which can lead to many frustrating
447 recordings from unconnected pairs of neurons. One way to address this is to increase the
448 numbers of recording pipettes to allow the testing of more connections per recording session
449 (Peng et al., 2017; Perin et al., 2011). Another could be to use transsynaptic tracing to visulaise
450 connected pairs of neurons prior to recording (Wickersham et al., 2007). So far, however,
451 single cell initiated transsynaptic tracing has been used with sequential rather than
452 simultaneous anatomical tracing (Vélez-Fort et al., 2018), or calcium imaging (Wertz et al.,
453 2015) of presynaptic neurons. With the use of less toxic rabies virus variants (Ciabatti et al.,
454 2017), this approach could now be attempted with simultaneous whole-cell recordings from
455 pre- and post-synaptic neurons.

456 To understand synaptic integration, it will be important to be able to activate unitary
457 inputs from more than 1 neuron with high temporal precision. The recent development of in
458 vivo single cell optogenetic stimulation (Packer et al., 2015; Rickgauer et al., 2014), has
459 provided a way to activate multiple single neurons with different spatial and temporal patterns.
460 A combination of this technique with in vivo whole-cell recording to monitor small amplitude
461 subthreshold synaptic inputs, could provide an exciting avenue to investigate the computations
462 underlying the integration of multiple unitary inputs in single cells.

463 An in vivo patch clamp recording session can be slow, especially when learning the
464 technique or using multiple electrodes. In particular the replacement of old pipettes with

465 unused ones at each new recording attempt takes up valuable time. A recent study has
466 circumvented this problem with the use of a commercially available detergent and rinsing
467 procedure (Kolb et al., 2016). This allowed the reuse of the same pipettes with no degradation
468 in signal fidelity both in vitro and in vivo. Robotic assistance to move the pipettes also may
469 help speed up this process and has recently been implemented for the entire visualised
470 patching process (Annecchino et al., 2017; Suk et al., 2017).
471 The craniotomy and glass recording pipette exposes the brain and requires the use of
472 extracellular Ringer's solution as well as an intracellular solution. These solutions are made in
473 the lab and therefore provide an access point for the application of extra- and intra-cellular
474 pharmacological agents in vivo. For example, we recently applied intracellular blockers of
475 different ion channels via the intracellular solution to investigate their impact on synaptic
476 integration during network activity (Ferrarese et al., 2018), and extracellular antagonist to
477 monitor the impact of acetylcholine on monosynaptic excitatory transmission between PYR
478 neurons and neighbouring SST GABA-ergic neurons (Urban-Ciecko et al., 2018). Future work
479 could therefore use specific pharmacological agents to help understand the ionic mechanisms
480 of synaptic transmission in active, intact networks.
481
482 **Conclusions**
483 Two-photon targeted multiple-whole cell recordings provide a high resolution and cell-type
484 specific way of identifying monosynaptically connected neurons *in vivo*. This approach will
485 allow studies into the impact of network activity on synaptic transmission and the synaptic
486 mechanisms underlying action potentials generation. Moreover, the possibility to record the V_m
487 of both pre- and post-synaptic neurons now provides a way to examine the synaptic basis of
488 correlated spiking activity of cortical neurons.
489
490 **AUTHORS CONTRIBUTIONS**
491 JSJ performed the experiments and analysed the data. JSJ and JFAP designed the study and
492 wrote the manuscript.
493
494 **ACKNOWLEDGMENTS**
495 We would like to thank Janett König for the technical assistance, Mario Carta, Sylvain Crochet,
496 Alison Barth and Evgeny Bobrov for comments on earlier version of the manuscript. We thank
497 the lab members for help and constructive comments. Finally, we would like to thank
498 Femtonics for technical assistance in setting up the 2-photon microscope for in vivo imaging.
499 This work was funded by the European Research Council (ERC-2010-StG-260590, ERC-
500 2015-CoG-682422, J.F.A.P.), the European Union (3x3Dimaging 323945), the Deutsche
501 Forschungsgemeinschaft (DFG, Exc 257 NeuroCure, FOR 1341, FOR 2143, J.F.A.P), the

American National Institute of Health (NIH R01NS088958, J.F.A.P.), the Thyssen Foundation (J.F.A.P.), and the Helmholtz Society (J.F.A.P.).

FIGURES

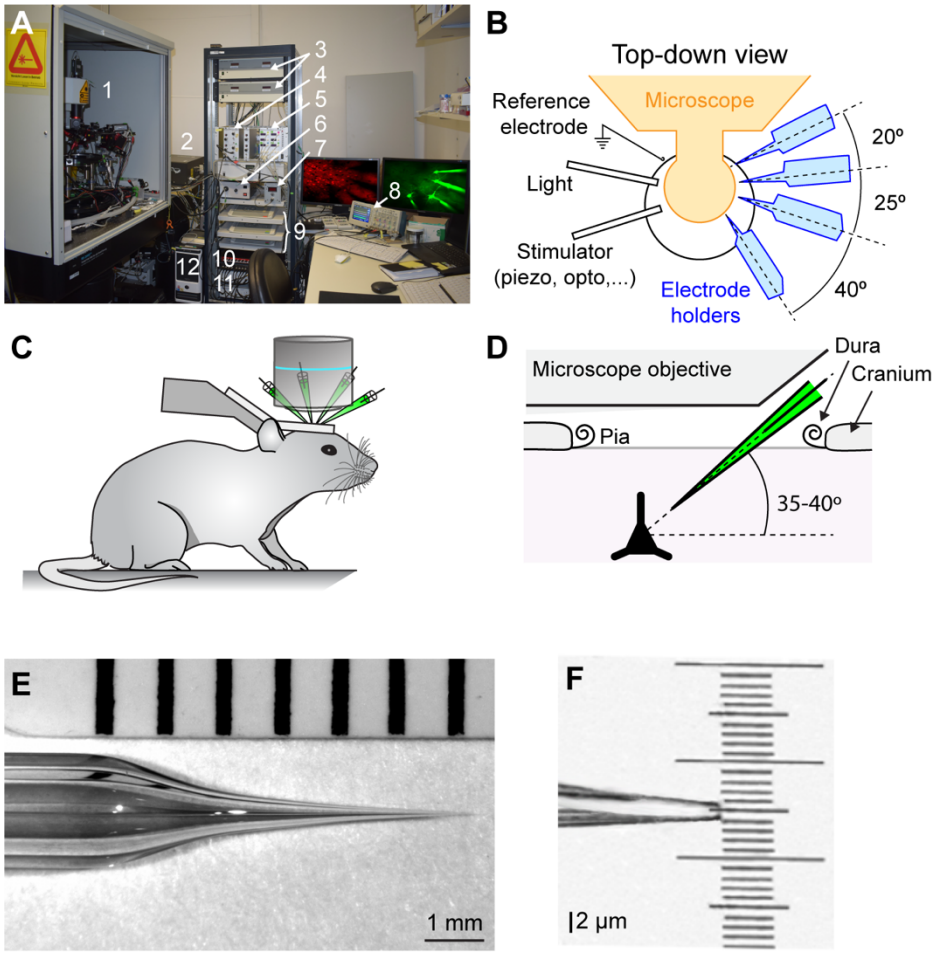

Figure 1. In vivo two-photon targeted multiple whole-cell patch-clamp setup.

(A) Photograph of the setup showing (1) Two-photon microscope, micromanipulators and pre-amplifier fixed on an air-damped table; (2) Chameleon Ultra II laser; (3) Luigs and Neumann micromanipulator control units; (4): Sigmann Electronik air pressure controller; (5) Sigmann Electronik dual piezo amplifier (6) Light source to illuminate the preparation, (7) FHC temperature controller, (8) Tektronix Oscilloscope, (9) Luigs and Neumman micromanipulator and shifting table control pads, (10) ITC-18 Heka analogue to digital converter board; (11) Multiclamp 700B amplifier; (12) Data acquisition computer.

(B) Schematic top-down view of recording area showing arrangement of electrode holders, light, reference electrode and somatosensory/optogenetic stimulator.

(C) Cartoon showing mouse position and head support.

(D) Schematic showing the angle of pipettes defined by the X-axis used to allow access under the objective.

(E) Photograph of the glass recording pipette showing optimal taper for two-photon targeted patch-clamp recording.

(F) Photograph showing a zoom of the pipette tip from (E).

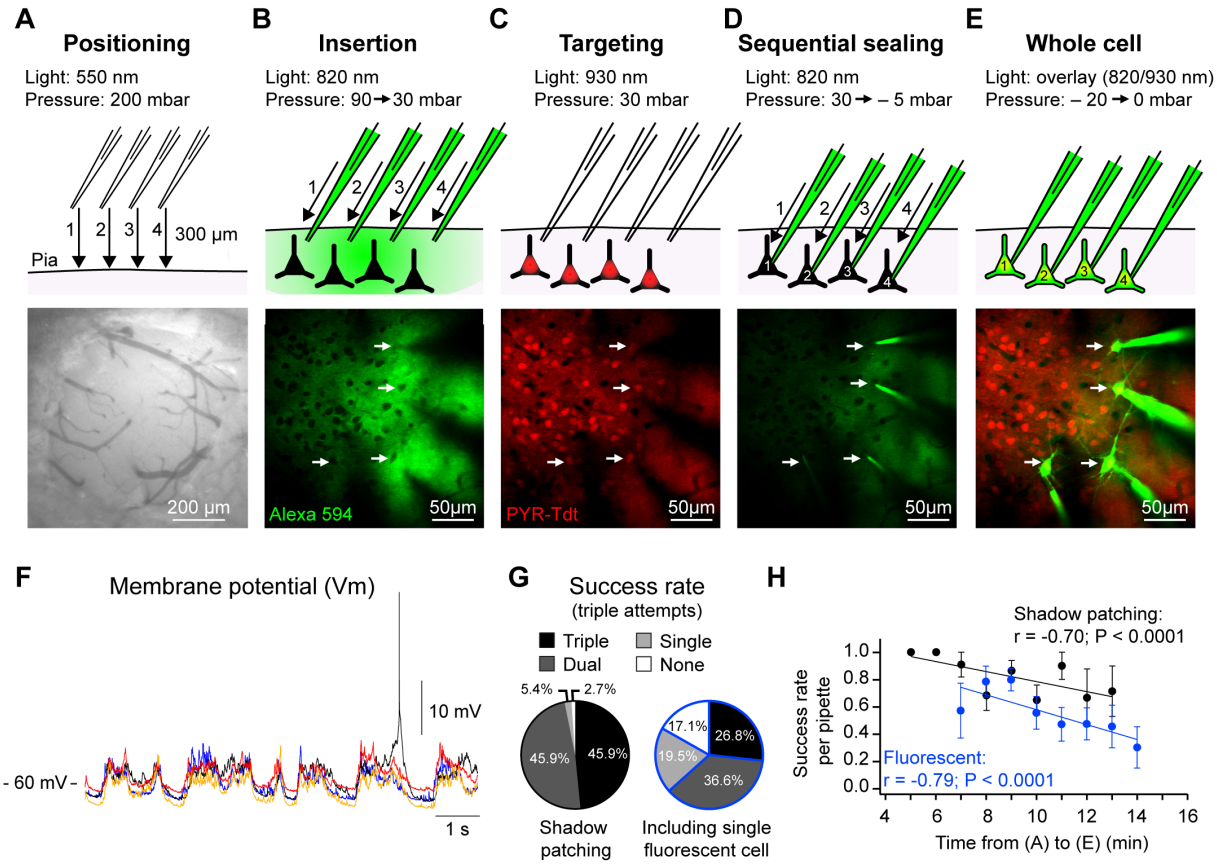

Figure 2. Two-photon targeted whole-cell patch-clamp procedure.

(A) Top: Schematic showing position, movement direction (arrow) and movement order (1-4) of dye-filled (Alexa 594) recording pipettes from ~ 300 µm above the craniotomy to the brain surface, high positive pressure is maintained to avoid pipette tip clogging. Bottom: photograph taken using a CCD camera illuminated with green light showing example craniotomy used for anesthetised patching (~ 500 µm diameter) in which the dura has been removed.

(B) As in (A), but showing, top: the insertion of the pipettes through the pia under visual control (820 nm) using high positive pressure to ~ – 100µm from pial surface. As soon as the pipettes enter the brain the pressure is reduced to 100 mbar and then 30 mbar when closer to the cell body positions. Bottom: In vivo two-photon image showing the position of 4 pipettes in same focal plan near the cell bodies of interest. Positioning is performed sequentially, one pipette at a time. Cell bodies are revealed as dark shadows contrasting with the fluorescent signal of the extracellular dye.

(C) Top: the targeting phase where the excitation light wavelength is altered to visualize the cells of interest; in this case, excitatory glutamatergic neurons expressing the red fluorophore tdT (white arrows). Bottom: in vivo fluorescent image of pyramidal neurons expressing tdT corresponding to the photo in (B).

(D) Top: the final sealing phase of the procedure. A recording pipette is pushed into the cell soma membrane and then, upon strong contact, the pressure is released to achieve a giga-seal. The cells are sealed sequentially under visual control. Bottom: in vivo image following

545 sealing of all 4 pipettes. Note the reduction in background fluorescence during sealing because
546 of the reduction in extracellular dye.
547 **(E)** Top: entering whole-cell configuration following seal-breaking by applying a transient
548 negative pressure. As soon as the membrane patch is ruptured the dye within the pipettes will
549 fill the neurons revealing anatomy. Bottom: in vivo image of neurons filled with Alexa 594 after
550 the recording experiments.
551 **(F)** Simultaneous example in vivo whole-cell V_m recordings of the four excitatory pyramidal
552 neurons shown in (E) showing spontaneous activity with Up- and Downstates under urethane
553 anaesthesia.
554 **(G)** Proportion of triple, double, single and no recordings from trials using three pipettes in (left)
555 wild type mice using the shadow patching method and (right) in mice expressing a cell type
556 specific fluorophore (PV x Ai9 and SST x Ai9). Data from fluorescent mice included at least 1
557 fluorescent neuron in the single/double/triple recordings.
558 **(H)** Plots showing the negative correlation between the success rate of achieving a whole-cell
559 patch clamp recording in wild type and fluorescent mice (same data as in (G)) and the time
560 taken from phases (A) to (E) described above. Each dot represents the mean success rate for
561 a 1 min time bin from 15 wild type mice (37 trials) and 18 mice expressing fluorescent proteins
562 (SST-cre x Ai9 and PV-crex Ai9; 42 trials).
563

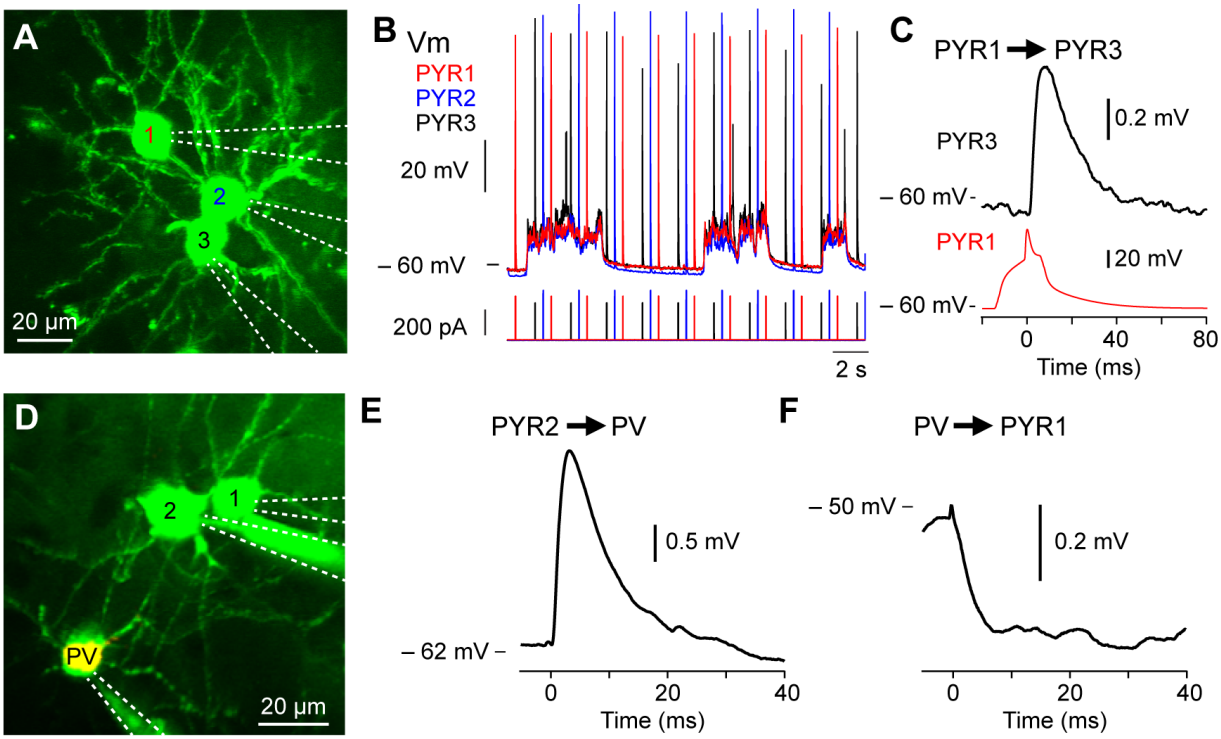

Figure 3: Example of monosynaptic connections in vivo.

(A) in vivo two-photon fluorescent imaging of three filled with Alexa 594 excitatory pyramidal neurons.

(B) Membrane potential fluctuation of the pyramidal neurons recoded in (A) showing the stimulation protocol consisting of brief current injection to evoke a single action potential in each neuron every 2 seconds.

(C) Example monosynaptic excitatory connection from neuron PYR1 to the neuron PYR3 shown in (A) and (B).

(D) In vivo image of a triple recording including a PV-tdT expressing interneuron.

(E) Excitatory monosynaptic connection from presynaptic neuron PYR2 and the PV interneurons from experiment shown in (D).

(F) Inhibitory monosynaptic connection from presynaptic PV expressing interneurons to the postsynaptic excitatory PYR1 neuron shown in (D).

583 **Table 1: Troubleshooting during multiple whole cell patching**

Step	Problem	Possible reason	Solution
Surgery	Edema	Brain surface damaged	Take care when removing the dura as damaging the pia will result in tissue swelling.
		Craniotomy too large	Keep size <1mm^2
		Anesthesia	Isoflurane increases plasma volume which can induce swelling (Hamada et al., 1993). Drill a smaller craniotomy and use 1.2% agarose in Ringer's solution on the craniotomy to damp the swelling. Or use urethane which does not increase plasma volume as much.
2	Pipettes unable to enter the brain	Dura intact	Re-attempt to remove the dura.
		Blood vessel in the way	Make sure your brain entry point is clear. The use of green light will help to increase the contrast between blood vessel and brain tissue.
3	Dye not flowing out the pipette	Pipette clogged	Make sure the positive pressure is on before entering the ringer solution this will help maintaining a clean pipette tip. Fresh pipette.
		Debris accumulating outside the pipette tip	Precipitate accumulating outside of the pipette could be a sign of grounding issue. Make sure the Ringer's solution in the recording chamber is not touching the head post.
		Pipette clogged, visible debris inside the pipette	Debris inside the pipette can come from the intracellular solution itself. Use a fresh 0.45 µm syringe filter (Minisart SRP4, Sartorius Stedium) for each experiment. Debris can also come from the silver chloride electrode. Make sure the end of the pipettes are flame polished to avoid removing pieces of silver chloride coating. Try clearing the tip of the pipette by increasing briefly the pressure (+ 50 mbar). If unsuccessful use new pipettes. Do not carry on with clogged pipettes even if the tip resistance is acceptable as it will most likely impair sealing.
		Faulty pressure system	Check air pressure system can maintain a stable pressure.
	No image	Laser off	Turn laser on.
		Shutter closed	Open shutter.
		PMT overload	Check external lights are switched off while the PMT's are on. Reset PMT.
	Poor imaging quality	High background fluorescence	Decrease the internal pipette pressure to reduce efflux of intracellular solution.
		Leak of Ringer's solution out of the recording chamber	Check the contact between Ringer's solution and the objective. Try fixing leak with Vaseline.
		Laser power is to high	Small spherical dark spots appearing in the image is a sign of tissue damage caused by high laser power. The quality of the preparation is compromised and experiment should be terminated.
4	Unable to seal	Pipette resistance not optimal	Although lower resistance pipette (< 5 MΩ) will give you a better access to the cell it can also decrease sealing success. Aim for pipette resistance of 5 – 8 MΩ.
		Dirt on pipette tip	Although the resistance of the dirty pipette tip might be in the expected range they will dramatically reduce chances to seal successfully on neurons. Fresh pipettes.
		Pressure while approaching the cell of interest	Decrease the pressure while approaching the cell. High pressure will tend to "push" away the targeted neuron. In addition, a slight negative pressure while sealing on the cell might be beneficial but also fatal.
		Intracellular solution	Check the osmolarity of your internal solution which usually need to be lower than the one of the Ringer's solution.
		Holding potential not set to -70 mV	Make sure the holding potential is set up to -70 mV while sealing on the cell. In some cases, it will help to bring gradually the cell to -100 mV during the sealing procedure and then holding it back to -70 mV before breaking in.

5	Unable to break in	Pipette resistance is too high	Pipette with a higher resistance than 8MΩ will tend to be more difficult to break in. The optimum pipette tip resistance is between 5 to 8 MΩ.
		Patched a blood vessel	On the same focal plan blood vessel might look like cell bodies. A quick up-down scan will usually help identifying clearly cells from capillaries. Fresh pipette.
		Patched on buddle of fibres	In some cases, the pipette might catch on fibres on the way to the cells of interest and even though a giga-seal will be made breaking in will fail. Fresh pipette.
		Faulty pressure system	Make sure the pressure system is reactive to your suction. Suction must be brief. If something is damping the change of pressure breaking in will be impaired.
Recording	Short duration recordings (<5 mins)	Brain movement	Breathing of the mouse might create movement. Check the position of the mouse head relative to the body. If movement persist use 1.2% agarose ringer solution to stabilise the brain movements, or stop the experiment. The pressure due to multiple pipettes entering the brain need to be accounted for. Eventually, the tissue will relax and "move back" to its original position which will create tension on the seal between the cell and the pipette. Visual check using two-photon scanning during the recording is valuable to adjust the pipette position in regard to the recorded neurons. New experiment with different anaesthesia.
		Craniotomy is too large	New experiment with smaller craniotomy.
		Unstable head implant	In case of chronic experiment it is possible that the head implant may loosened due to tissue regrowth or poor gluing.
		Location of the pipette relative to the cell of interest	Aim for the most dorsal third of the targeted neuron soma to increase success rate and stability.
	Unable to trigger action potentials	Patched on glial cell	Check firing pattern, glial cells do not spike and typically have a very hyperpolarized V_m with no spontaneous activity. Change pipette and start over.
		Access resistance is too high	Try to gain better access by transiently applying negative pressure to the pipette tip.
	V_m depolarized	Recording solution	Use fresh Ringer's and intracellular solutions with correct osmolarity.
	V_m drift	Reference electrodes	Change or re-chloridize the recording and reference electrodes.
		Metal head implant touching Ringer's solution	Isolate head implant from Ringer's solution in recording chamber.
	No spontaneous activity	Anaesthesia level too high	Reduce isoflurane levels.
		Body temperature is too low	Check the temperature of the mouse and feedback controller.

REFERENCES

Annecchino, L. A., Morris, A. R., Copeland, C. S., Agabi, O. E., Chadderton, P., and Schultz, S. R. (2017). Robotic Automation of In Vivo Two-Photon Targeted Whole-Cell Patch-Clamp Electrophysiology. *Neuron* 95, 1048–1055.e3. doi:10.1016/j.neuron.2017.08.018.

Arroyo, S., Bennett, C., and Hestrin, S. (2018). Correlation of Synaptic Inputs in the Visual Cortex of Awake, Behaving Mice. *Neuron* 99, 1289–1301.e2. doi:10.1016/j.neuron.2018.08.008.

Barry, P. H., and Lynch, J. W. (1991). Liquid junction potentials and small cell effects in patch-clamp analysis. *J. Membr. Biol.* 121, 101–117.

Barth, A. L., Gerkin, R. C., and Dean, K. L. (2004). Alteration of neuronal firing properties after in vivo experience in a FosGFP transgenic mouse. *J. Neurosci.* 24, 6466–6475. doi:10.1523/JNEUROSCI.4737-03.2004.

Bartho, P. (2004). Characterization of Neocortical Principal Cells and Interneurons by Network Interactions and Extracellular Features. *J. Neurophysiol.* 92, 600–608. doi:10.1152/jn.01170.2003.

Berry, M. S., and Pentreath, V. W. (1976). Criteria for distinguishing between monosynaptic and polysynaptic transmission. *Brain Res.* 105, 1–20.

Bruno, R. M. (2006). Cortex Is Driven by Weak but Synchronously Active Thalamocortical Synapses. *Science* 312, 1622–1627. doi:10.1126/science.1124593.

Burrows, M. (1996). *The Neurobiology of an Insect Brain*. Oxford University Press. Oxford University Press doi:10.1093/acprof:oso/9780198523444.001.0001.

Ciabatti, E., González-Rueda, A., Mariotti, L., Morgese, F., and Tripodi, M. (2017). Life-Long Genetic and Functional Access to Neural Circuits Using Self-Inactivating Rabies Virus. *Cell* 170, 382–392.e14. doi:10.1016/j.cell.2017.06.014.

Crochet, S., Chauvette, S., Boucetta, S., and Timofeev, I. (2005). Modulation of synaptic transmission in neocortex by network activities. *Eur. J. Neurosci.* 21, 1030–1044. doi:10.1111/j.1460-9568.2005.03932.x.

Csicsvari, J., Hirase, H., Czurko, A., and Buzsaki, G. (1998). Reliability and state dependence of pyramidal cell-interneuron synapses in the hippocampus: an ensemble approach in the behaving rat. *Neuron* 21, 179–189.

Daigle, T. L., Madisen, L., Hage, T. A., Valley, M. T., Knoblich, U., Larsen, R. S., et al. (2018). A Suite of Transgenic Driver and Reporter Mouse Lines with Enhanced Brain-Cell-Type Targeting and Functionality. *Cell* 174, 465–480.e22. doi:10.1016/j.cell.2018.06.035.

Destexhe, A., Rudolph, M., and Paré, D. (2003). The high-conductance state of neocortical neurons in vivo. *Nat Rev Neurosci* 4, 739–751. doi:10.1038/nrn1198.

Deuchars, J., and Thomson, A. M. (1995). Innervation of burst firing spiny interneurons by pyramidal cells in deep layers of rat somatomotor cortex: paired intracellular recordings with biocytin filling. *Neuroscience* 69, 739–755.

Edwards, F. A., Konnerth, A., Sakmann, B., and Takahashi, T. (1989). A thin slice preparation for patch clamp recordings from neurones of the mammalian central nervous system. *Pfl□gers Archiv European Journal of Physiology* 414, 600–612.

English, D. F., McKenzie, S., Evans, T., Kim, K., Yoon, E., and Buzsáki, G. (2017). Pyramidal Cell-Interneuron Circuit Architecture and Dynamics in Hippocampal Networks. *Neuron* 96, 505–520.e7. doi:10.1016/j.neuron.2017.09.033.

Feldmeyer, D., and Radnikow, G. (2016). "Paired Recordings from Synaptically Coupled Neurones in Acute Neocortical Slices," in *Advanced Patch-Clamp Analysis for Neuroscientists* Neuromethods. (New York, NY: Springer New York), 171–191. doi:10.1007/978-1-4939-3411-9_9.

Feldmeyer, D., Lübke, J., and Sakmann, B. (2006). Efficacy and connectivity of intracolumnar pairs of layer 2/3 pyramidal cells in the barrel cortex of juvenile rats. *J. Physiol. (Lond.)* 575, 583–602. doi:10.1113/jphysiol.2006.105106.

Ferrarese, L., Jouhanneau, J.-S., Remme, M. W. H., Kremkow, J., Katona, G., Rózsa, B., et al. (2018). Dendrite-Specific Amplification of Weak Synaptic Input during Network Activity In Vivo. *Cell Rep* 24, 3455–3465.e5. doi:10.1016/j.celrep.2018.08.088.

Fujisawa, S., Amarasingham, A., Harrison, M. T., and Buzsáki, G. (2008). Behavior-dependent short-term assembly dynamics in the medial prefrontal cortex. *Nat. Neurosci.* 11, 823–833. doi:10.1038/nn.2134.

Geiger, J. R., Lübke, J., Roth, A., Frotscher, M., and Jonas, P. (1997). Submillisecond AMPA receptor-mediated signaling at a principal neuron-interneuron synapse. *Neuron* 18, 1009–1023.

Gentet, L. J., Avermann, M., Matyas, F., Staiger, J. F., and Petersen, C. C. H. (2010). Membrane potential dynamics of GABAergic neurons in the barrel cortex of behaving mice. *Neuron* 65, 422–435. doi:10.1016/j.neuron.2010.01.006.

Gerfen, C. R., Paletzki, R., and Heintz, N. (2013). GENSAT BAC cre-recombinase driver lines to study the functional organization of cerebral cortical and basal ganglia circuits. *Neuron* 80, 1368–1383. doi:10.1016/j.neuron.2013.10.016.

Goebbels, S., Bormuth, I., Bode, U., Hermanson, O., Schwab, M. H., and Nave, K.-A. (2006). Genetic targeting of principal neurons in neocortex and hippocampus of NEX-Cre mice. *genesis* 44, 611–621. doi:10.1002/dvg.20256.

Guzman, S. J., Schlögl, A., Frotscher, M., and Jonas, P. (2016). Synaptic mechanisms of pattern completion in the hippocampal CA3 network. *Science* 353, 1117–1123. doi:10.1126/science.aaf1836.

Hamada, H., Takaori, M., Kimura, K., Fukui, A., and Fujita, Y. (1993). Changes in circulating blood volume following isoflurane or sevoflurane anesthesia. *J Anesth* 7, 316–324. doi:10.1007/s0054030070316.

Harris, J. A., Hirokawa, K. E., Sorensen, S. A., Gu, H., Mills, M., Ng, L. L., et al. (2014). Anatomical characterization of Cre driver mice for neural circuit mapping and manipulation. *Front. Neural Circuits* 8, 76. doi:10.3389/fncir.2014.00076.

Hippenmeyer, S., Vrieseling, E., Sigrist, M., Portmann, T., Laengle, C., Ladle, D. R., et al. (2005). A developmental switch in the response of DRG neurons to ETS transcription factor signaling. *PLoS Biol.* 3, e159. doi:10.1371/journal.pbio.0030159.

Holmgren, C., Harkany, T., Svennenfors, B., and Zilberter, Y. (2003). Pyramidal cell communication within local networks in layer 2/3 of rat neocortex. *J. Physiol. (Lond.)* 551, 139–153. doi:10.1113/jphysiol.2003.044784.

671 Jouhanneau, J.-S., Kremkow, J., and Poulet, J. F. A. (2018). Single synaptic inputs drive
672 high-precision action potentials in parvalbumin expressing GABA-ergic cortical neurons
673 in vivo. *Nat Commun* 9, 1540. doi:10.1038/s41467-018-03995-2.

674 Jouhanneau, J.-S., Kremkow, J., Dorrn, A. L., and Poulet, J. F. A. (2015). In Vivo
675 Monosynaptic Excitatory Transmission between Layer 2 Cortical Pyramidal Neurons.
676 *Cell Rep* 13, 2098–2106. doi:10.1016/j.celrep.2015.11.011.

677 Kitamura, K., Judkewitz, B., Kano, M., Denk, W., and Häusser, M. (2008). Targeted patch-
678 clamp recordings and single-cell electroporation of unlabeled neurons in vivo. *Nat.*
679 *Methods* 5, 61–67. doi:10.1038/nmeth1150.

680 Kolb, I., Stoy, W. A., Rousseau, E. B., Moody, O. A., Jenkins, A., and Forest, C. R. (2016).
681 Cleaning patch-clamp pipettes for immediate reuse. *Sci Rep* 6, 35001.
682 doi:10.1038/srep35001.

683 Lalanne, T., Abrahamsson, T., and Sjöström, P. J. (2016). Using Multiple Whole-Cell
684 Recordings to Study Spike-Timing-Dependent Plasticity in Acute Neocortical Slices. *Cold*
685 *Spring Harb Protoc* 2016, pdb.prot091306. doi:10.1101/pdb.prot091306.

686 Lee, A. K., and Brecht, M. (2018). Elucidating Neuronal Mechanisms Using Intracellular
687 Recordings during Behavior. *Trends in Neurosciences* 41, 385–403.
688 doi:10.1016/j.tins.2018.03.014.

689 Lefort, S., and Petersen, C. C. H. (2017). Layer-Dependent Short-Term Synaptic Plasticity
690 Between Excitatory Neurons in the C2 Barrel Column of Mouse Primary Somatosensory
691 Cortex. *Cereb. Cortex* 27, 3869–3878. doi:10.1093/cercor/bhx094.

692 Lefort, S., Tomm, C., Sarria, J. C. F., and Petersen, C. C. H. (2009). The Excitatory Neuronal
693 Networkof the C2 Barrel Columnin Mouse Primary Somatosensory Cortex. *Neuron* 61,
694 301–316. doi:10.1016/j.neuron.2008.12.020.

695 London, M., Roth, A., Beeren, L., Häusser, M., and Latham, P. E. (2010). Sensitivity to
696 perturbations in vivo implies high noise and suggests rate coding in cortex. *Nature* 466,
697 123–127. doi:10.1038/nature09086.

698 Madisen, L., Zwingman, T. A., Sunkin, S. M., Oh, S. W., Zariwala, H. A., Gu, H., et al. (2010).
699 A robust and high-throughput Cre reporting and characterization system for the whole
700 mouse brain. *Nat. Neurosci.* 13, 133–140. doi:10.1038/nn.2467.

701 Margrie, T., Brecht, M., and Sakmann, B. (2002). In vivo, low-resistance, whole-cell
702 recordings from neurons in the anaesthetized and awake mammalian brain. *Pfl□gers*
703 *Archiv European Journal of Physiology* 444, 491–498. doi:10.1007/s00424-002-0831-z.

704 Markram, H., Lübke, J., Frotscher, M., Roth, A., and Sakmann, B. (1997). Physiology and
705 anatomy of synaptic connections between thick tufted pyramidal neurones in the
706 developing rat neocortex. *J. Physiol. (Lond.)* 500 (Pt 2), 409–440.

707 Mason, A., Nicoll, A., and Stratford, K. (1991). Synaptic transmission between individual
708 pyramidal neurons of the rat visual cortex in vitro. *J. Neurosci.* 11, 72–84.

709 Matsumura, M., Chen, D., Sawaguchi, T., Kubota, K., and Fetz, E. E. (1996). Synaptic
710 interactions between primate precentral cortex neurons revealed by spike-triggered
711 averaging of intracellular membrane potentials in vivo. *J. Neurosci.* 16, 7757–7767.

Packer, A. M., Russell, L. E., Dalgleish, H. W. P., and Häusser, M. (2015). Simultaneous all-optical manipulation and recording of neural circuit activity with cellular resolution in vivo. *Nat. Methods* 12, 140–146. doi:10.1038/nmeth.3217.

Pala, A., and Petersen, C. C. (2018). State-dependent cell-type-specific membrane potential dynamics and unitary synaptic inputs in awake mice. *eLife* 7, 350. doi:10.7554/eLife.35869.

Pala, A., and Petersen, C. C. H. (2014). In Vivo Measurement of Cell-Type-Specific Synaptic Connectivity and Synaptic Transmission in Layer 2/3 Mouse Barrel Cortex. *Neuron* 85, 68–75. doi:10.1016/j.neuron.2014.11.025.

Papadopoulos, I. N., Jouhanneau, J.-S., Poulet, J. F. A., and Judkewitz, B. (2017). Scattering compensation by focus scanning holographic aberration probing (F-SHARP). *Nature Photonics 2016 11:2* 11, 116–123. doi:10.1038/nphoton.2016.252.

Parker, D. (2003). Variable properties in a single class of excitatory spinal synapse. *J. Neurosci.* 23, 3154–3163.

Parker, D. (2010). Neuronal network analyses: premises, promises and uncertainties. *Philosophical Transactions of the Royal Society B: Biological Sciences* 365, 2315–2328. doi:10.1038/nature05744.

Peng, Y., Barreda Tomás, F. J., Klisch, C., Vida, I., and Geiger, J. R. P. (2017). Layer-Specific Organization of Local Excitatory and Inhibitory Synaptic Connectivity in the Rat Presubiculum. *Cereb. Cortex* 27, 2435–2452. doi:10.1093/cercor/bhx049.

Perin, R., Berger, T. K., and Markram, H. (2011). A synaptic organizing principle for cortical neuronal groups. *Proc. Natl. Acad. Sci. U.S.A.* 108, 5419–5424. doi:10.1073/pnas.1016051108.

Petersen, C. C. H. (2017). Whole-Cell Recording of Neuronal Membrane Potential during Behavior. *Neuron* 95, 1266–1281. doi:10.1016/j.neuron.2017.06.049.

Poulet, J. F. A., and Hedwig, B. (2006). The cellular basis of a corollary discharge. *Science* 311, 518–522. doi:10.1126/science.1120847.

Poulet, J. F. A., and Petersen, C. C. H. (2008). Internal brain state regulates membrane potential synchrony in barrel cortex of behaving mice. *Nature* 454, 881–885. doi:10.1038/nature07150.

Reid, R. C., and Alonso, J. M. (1995). Specificity of monosynaptic connections from thalamus to visual cortex. *Nature* 378, 281–284. doi:10.1038/378281a0.

Reig, R., Zerlaut, Y., Vergara, R., Destexhe, A., and Sanchez-Vives, M. V. (2015). Gain modulation of synaptic inputs by network state in auditory cortex in vivo. *J. Neurosci.* 35, 2689–2702. doi:10.1523/JNEUROSCI.2004-14.2015.

Rickgauer, J. P., Deisseroth, K., and Tank, D. W. (2014). Simultaneous cellular-resolution optical perturbation and imaging of place cell firing fields. *Nat. Neurosci.* 17, 1816–1824. doi:10.1038/nn.3866.

Roberts, A., Li, W.-C., and Soffe, S. R. (2010). How neurons generate behavior in a hatchling amphibian tadpole: an outline. *Front Behav Neurosci* 4, 16. doi:10.3389/fnbeh.2010.00016.

Sofroniew, N. J., Flickinger, D., King, J., and Svoboda, K. (2016). A large field of view two-photon mesoscope with subcellular resolution for in vivo imaging. *eLife* 5, 413. doi:10.7554/eLife.14472.

Steriade, M., Nuñez, A., and Amzica, F. (1993). A Novel Slow (<1 Hz) Oscillation of Neocortical Neurons in viva: Depolarizing and Hyperpolarizing Components. *Journal of Neuroscience Methods* 13, 3252–3265.

Suk, H.-J., van Welie, I., Kodandaramaiah, S. B., Allen, B., Forest, C. R., and Boyden, E. S. (2017). Closed-Loop Real-Time Imaging Enables Fully Automated Cell-Targeted Patch-Clamp Neural Recording In Vivo. *Neuron* 96, 244–245. doi:10.1016/j.neuron.2017.09.012.

Swadlow, H. A., and Gusev, A. G. (2002). Receptive-field construction in cortical inhibitory interneurons. *Nat. Neurosci.* 5, 403–404. doi:10.1038/nn847.

Tamamaki, N., Yanagawa, Y., Tomioka, R., Miyazaki, J.-I., Obata, K., and Kaneko, T. (2003). Green fluorescent protein expression and colocalization with calretinin, parvalbumin, and somatostatin in the GAD67-GFP knock-in mouse. *J. Comp. Neurol.* 467, 60–79. doi:10.1002/cne.10905.

Taniguchi, H., He, M., Wu, P., Kim, S., Paik, R., Sugino, K., et al. (2011). NeuroResource. *Neuron* 71, 995–1013. doi:10.1016/j.neuron.2011.07.026.

Urban-Ciecko, J., Jouhanneau, J.-S., Myal, S. E., Poulet, J. F. A., and Barth, A. L. (2018). Precisely Timed Nicotinic Activation Drives SST Inhibition in Neocortical Circuits. *Neuron* 97, 611–625.e5. doi:10.1016/j.neuron.2018.01.037.

Vélez-Fort, M., Bracey, E. F., Keshavarzi, S., Rousseau, C. V., Cossell, L., Lenzi, S. C., et al. (2018). A Circuit for Integration of Head- and Visual-Motion Signals in Layer 6 of Mouse Primary Visual Cortex. *Neuron* 98, 179–191.e6. doi:10.1016/j.neuron.2018.02.023.

Wertz, A., Trenholm, S., Yonehara, K., Hillier, D., Raics, Z., Leinweber, M., et al. (2015). PRESYNAPTIC NETWORKS. Single-cell-initiated monosynaptic tracing reveals layer-specific cortical network modules. *Science* 349, 70–74. doi:10.1126/science.aab1687.

Wickersham, I. R., Lyon, D. C., Barnard, R. J. O., Mori, T., Finke, S., Conzelmann, K.-K., et al. (2007). Monosynaptic Restriction of Transsynaptic Tracing from Single, Genetically Targeted Neurons. *Neuron* 53, 639–647. doi:10.1016/j.neuron.2007.01.033.

Wozny, C., and Williams, S. R. (2011). Specificity of synaptic connectivity between layer 1 inhibitory interneurons and layer 2/3 pyramidal neurons in the rat neocortex. *Cereb. Cortex* 21, 1818–1826. doi:10.1093/cercor/bhq257.

Yassin, L., Benedetti, B. L., Jouhanneau, J.-S., Wen, J. A., Poulet, J. F. A., and Barth, A. L. (2010). An Embedded Subnetwork of Highly Active Neurons in the Neocortex. *Neuron* 68, 1043–1050. doi:10.1016/j.neuron.2010.11.029.

Yu, J., and Ferster, D. (2013). Functional coupling from simple to complex cells in the visually driven cortical circuit. *J. Neurosci.* 33, 18855–18866. doi:10.1523/JNEUROSCI.2665-13.2013.

Zhao, W.-J., Kremkow, J., and Poulet, J. F. A. (2016). Translaminar Cortical Membrane Potential Synchrony in Behaving Mice. *Cell Rep* 15, 1–34. doi:10.1016/j.celrep.2016.05.026.